a reprint from Applied Optics

New laser plasma source for extreme-ultraviolet lithography

F. Jin and M. Richardson

As the demands of lithographic fabrication of computer chips push toward ever-decreasing feature sizes, projection extreme-ultraviolet (EUV) lithography becomes an increasingly attractive technology. The radiation source of choice for this approach is a laser plasma with a high repetition rate. We report an investigation of a new candidate laser plasma source for EUV lithography that is based on line emission from ice-water targets. This radiation source has the potential to meet all the strict requirements of EUV conversion, debris elimination, operation, and cost for a demonstration lithographic system.

1. Introduction

Laser-produced plasmas hold great promise as bright sources of extreme-ultraviolet (EUV) radiation for applications such as projection lithography[1–3] and microscopy.[4] Recent advances in high repetition rate, high average power laser systems suggest the feasibility of modular, flexible, and relatively inexpensive microelectronics production facilities based on laser plasma sources.[5,6] The most formidable problem confronting the advancement of this technology is the design and experimental demonstration of a reliable, clean, and cheap target system that meets very stringent production-line criteria. In a production-line facility, the laser plasma target system should undergo uninterrupted, round-the-clock operation for at least 10^{10} shots (3 months at a 1-kHz repetition rate), depositing negligible debris (<10 nm) on nearby condenser optics, and the unit shot cost should be of the order of 10^{-6}. Conventional solid metal targets[5] pose extreme debris problems, and the level of debris ejected from thin-film-coated, tape-drive targets[7,8] is also unacceptable, even if interdiction measures are invoked. This type of target also has difficulties in meeting the cost requirements and in sustaining continuous operation.

We propose a new type of target, the mass-limited cryogenic target.[9] This type of target has only the mass that is necessary for forming the radiating plasma (it is mass limited) and exists in the gas phase at room temperature (it is cryogenic) in order to avoid condensation on the optics and for the pumping system to carry it away immediately after the laser shot. By constructing the target in such a way, we believe that the debris problem can be solved or at least reduced to the level of tolerance of the production line.

Several possible cryogenic target materials were suggested earlier in the literature.[6] Here we discuss targets of oxygen-containing compounds, because both helium-like and lithium-like oxygen ions have several strong emission lines near 13 nm.[10] This is the most favorable wavelength choice for projection lithography at the present time because of the availability of high reflectivity ($R > 65\%$) Mo–Si multilayer mirrors at this wavelength. Among the oxygen-containing compounds, the most interesting and cheapest one is H_2O in its liquid or solid phase. The preliminary experimental results of ice-water targets presented below show that this kind of target is indeed promising for solving the debris, material handling, and cost problems while keeping the x-ray conversion efficiency (CE) in a narrow band near 13 nm, comparable with that of a solid metal target.

We review the outstanding problems and practical requirements for a laser plasma source in Section 2. In Sections 3 and 4 we describe the issues of debris, material handling, and cost, and we make comparisons between conventional target systems and our water target system. Our latest calculation and experimental results on laser-produced ice plasmas are presented in Section 5. We summarize our findings in Section 6.

The authors are with the Center for Research and Education in Optics and Lasers, University of Central Florida, 12424 Research Parkway, Orlando, Florida 32826.

Received 4 October 1994; revised manuscript received 6 February 1995.

0003-6935/95/255750-11$06.00/0.

2. Laser Plasma Extreme Ultraviolet Emission

From the Ceglio and Hawryluk[11] prototype design of a projection lithography system, the throughput, T, of the system can be expressed as

$$T = \frac{R^7 W^3 (d\Omega/\pi)}{S} P_x,$$

$$P_x = \eta P_L,$$

where R is the peak reflectivity of a single multilayer mirror, W is the transmission of walls (thin-foil baffles) between different vacuum chambers, $d\Omega$ is the collecting solid angle, S is the resist sensitivity, P_x is the x-ray power within a 0.3-nm bandwidth from the laser-produced plasma, η is the x-ray CE to the narrow band, and P_L is the laser power. The 0.3-nm bandwidth is determined by the combined reflectivity of all the Mo–Si multilayer optics in the projection lithography system.

For a set of optimum parameters of $T = 2.5\ \mathrm{cm^2/s}$, $S = 2\ \mathrm{mJ/cm^2}$, $R = W = 60\%$, and $d\Omega/\pi = 10\%$, the minimum required x-ray power, P_x, within the bandwidth of the multilayer mirror is approximately 10 W. This corresponds to a 10-mJ x-ray energy per pulse for a laser repetition rate of 1 kHz, and to a CE of not less than 1% for a laser energy of 1 J per pulse. A CE of approximately 1% has already been demonstrated experimentally.[12]

High-Z solid targets, for example, those elements in the vicinity of Sn, characteristically emit broadband spectra that come from many excited levels of different ionization stages. These energy levels are so close that the radiation they generate in the EUV range can be considered as a continuum. The multilayer mirrors used in the collecting optical system, however, have high reflectivity only within a bandwidth of 0.3 nm centered around 13 nm. Thus most of the radiation from high-Z targets falls outside of this usable bandwidth (off-band radiation) and is absorbed by the coating materials on the mirror. The absorbed energy will heat the mirror and increase its surface temperature. For a high-repetition-rate lithography system, this temperature rise may cause thermal distortions of the multilayer structure and therefore reduce the reflectivity of the mirror.

Low-Z target materials such as oxygen, in contrast, generally emit simple line spectra in the EUV range. This results from the relatively small number of ion species and because the energy levels of these ions are sparsely distributed for the temperature of laser-produced plasmas. Thus if the narrow-band mirror reflectivity can be matched to this simple line spectra, the off-band heating problem of the broadband radiation could be reduced. Figure 1 is an energy diagram of lithium-like oxygen ions. It is noted that the strong transitions from $4d$ to $2p$ near 12.95 nm fall within the desired 0.3-nm bandwidth of the high-reflectivity Mo–Si mirrors of a projection lithography system; one of them has the oscillator strength of 0.124.[13] Here, we therefore concentrate on configurations that maximize emission from these transitions.

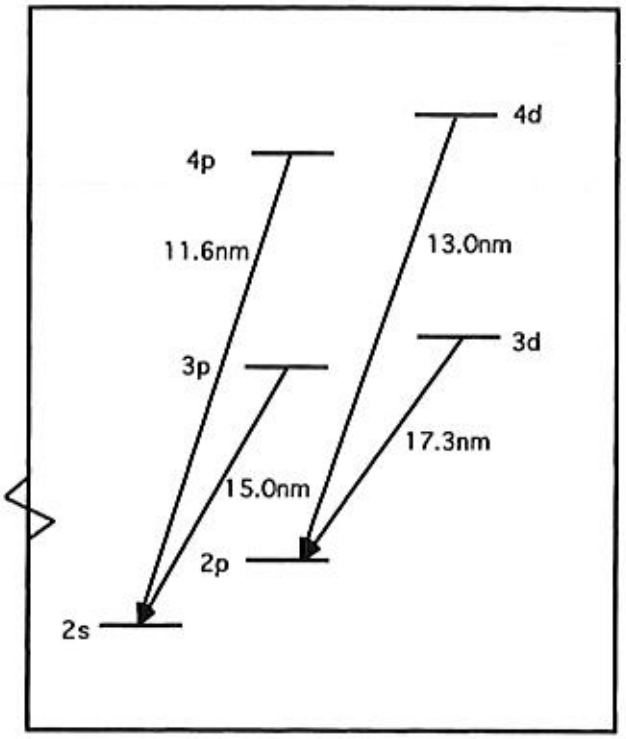

Fig. 1. Partial energy levels of Li-like oxygen.

There exist many types of oxygen-containing compounds that are potential target materials, such as SiO_2, CO_2, CuO, and H_2O. H_2O is probably the cheapest to obtain and also the easiest to handle. Another advantage of H_2O is that hydrogen has an ionization potential of 13.6 eV; thus the shortest line radiation from hydrogen is ~90 nm. Therefore the EUV radiation from this plasma will not be reabsorbed by hydrogen atoms on its passage through the plasma. This may not be true for plasmas from other oxygen-containing compounds, such as SiO_2. We present here both theoretical and experimental studies of H_2O targets, particularly for EUV lithography.

Several ionization stages of oxygen exist in the laser-produced plasma from an ice-water target. The relative populations of these ionization stages are a function of the electron temperature and density of the plasma, which themselves depend on the laser and target material parameters. Figures 2 and 3 show the calculated population distribution [14] of several oxygen ions and the ratio of the lithium-like $4d$ level population (n_{4d}) to the total number of oxygen ions, n_{total}, versus the electron temperature for three electron densities (n_e) of $10^{20}\ \mathrm{cm^{-3}}$, $10^{21}\ \mathrm{cm^{-3}}$, and $10^{22}\ \mathrm{cm^{-3}}$, respectively, with

$$n_{\mathrm{total}} = \sum_{i=1}^{8} n_i,$$

$$n_e = \sum_{i=1}^{8} i n_i = 10^{21}\ \mathrm{cm^{-3}},$$

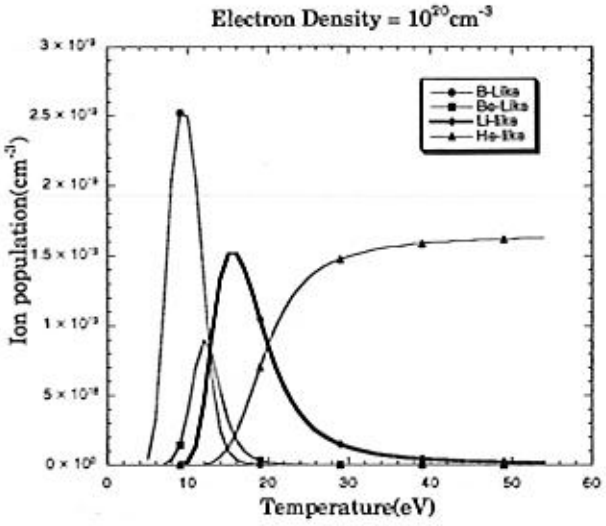

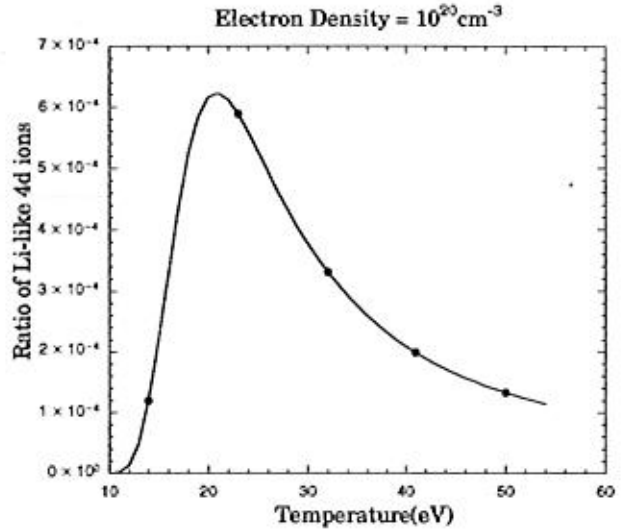

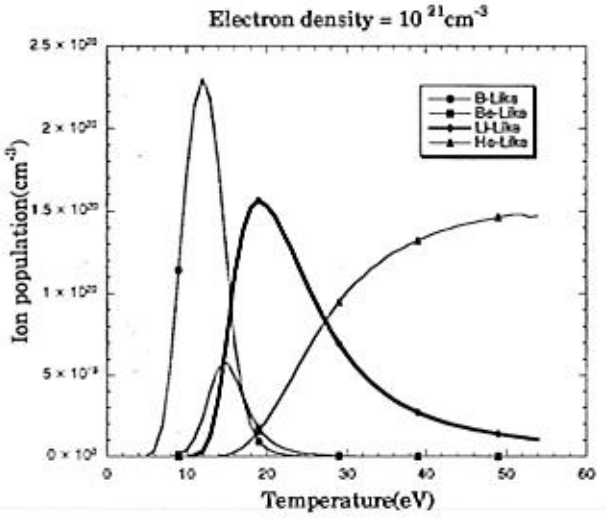

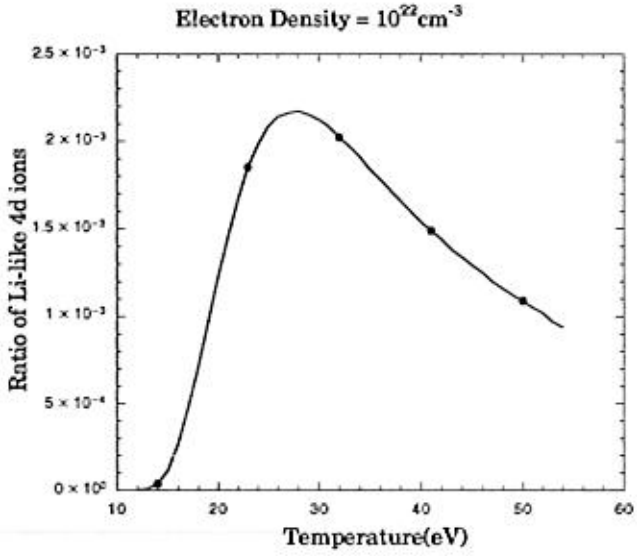

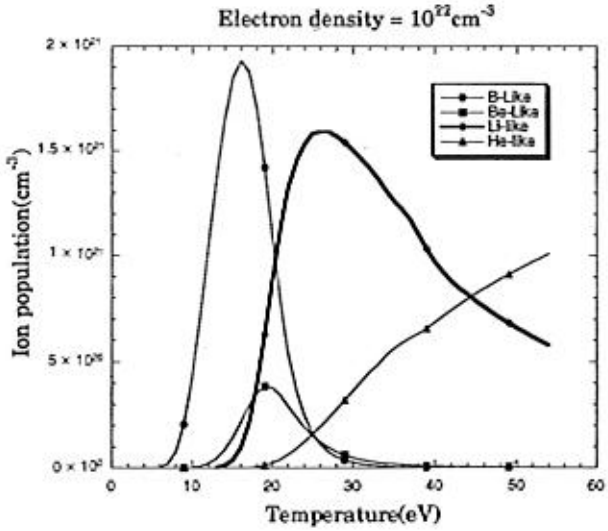

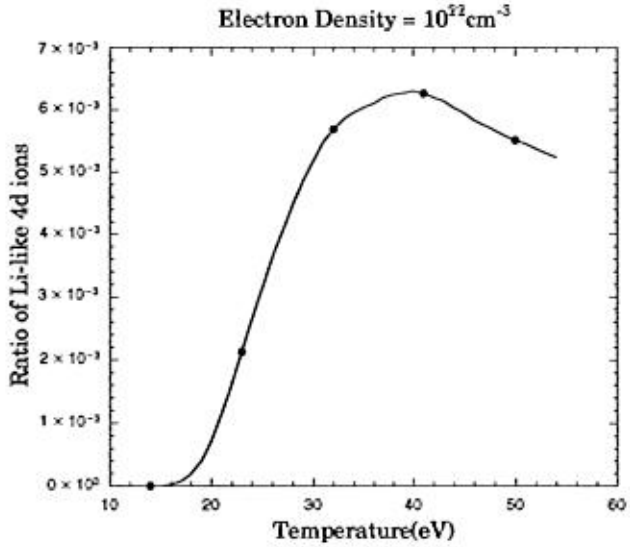

Fig. 2. Ion population for different electron densities.

Fig. 3. Ratio of Li-like ions for different electron densities.

where n_i is the number density in the ith ionization stage. To optimize the x-ray conversion efficiency, we find it necessary to select the laser and target material parameters in such a way that the lithiumlike ions (or more specifically the $4d$ level population of the lithiumlike ions) are dominant in the plasma. We note that a temperature of ~25 eV optimally populates to the desired energy levels in lithiumlike oxygen n_{4d}.

3. Target Debris

When a plasma is formed on the surface of a solid target by a focused high-power laser beam, part of the surface material expands and ablates in the form of high-velocity ions, electrons, and clusters. These particles can progressively coat the nearby x-ray condenser mirror of the collecting optics system and thereby reduce the mirror reflectivity by either increasing the absorption of the mirror surface to the incoming x-rays or by off-phasing the waves reflected from different layers of the mirror. In addition, the larger particles can also damage the mirror locally by transferring its kinetic energy to thermal energy at the impact site. It is believed that the coating effect is the major mechanism of x-ray mirror damage by debris for laser intensities of 10^{11}–10^{13} W/cm^2. The maximum coating thickness that can be tolerated to build up on the mirror depends on the EUV absorption of the target material used and the central x-ray wavelength at which the mirror reflectivity is peaked. High-Z materials will be greater EUV absorbers than low-Z materials. If we assume that the maximum tolerable buildup of material thickness can be less than a single mirror coating layer (~10 nm) over 10^{10} shots on a mirror situated at a distance of 20 cm from the target, and that all ions emitted from the target in the direction of the mirror reach this distance and stick to the mirror uniformly, then only ~10^{11} ions[5] or atoms from the solid target can be created per shot.

The number of photons radiated from the plasma must be approximately 6.5×10^{14} per pulse for the requirement of a 10-mJ x-ray flux within the 0.3-nm bandwidth centered at 13 nm. Assuming that individual ions radiate into this bandwidth only once during the course of a laser pulse, and that only a fraction (1%) of target atoms radiate into this bandwidth, we find that the minimum number of target atoms required for the desired x-ray energy is approximately 6.5×10^{16} per pulse.

Thus the minimum number of ions or atoms required to produce sufficient x rays is of the order of 10^{17} per pulse, whereas a flux of 10^{11} ions or atoms per pulse is enough to produce an unacceptable coating of the nearby mirrors on the assumption of 100% sticking efficiency. From this we deduce that for such a laser target system, only one in 10^6 radiated target atoms can be allowed to hit the mirror. This is a great challenge for any conventional solid target design. Several measures have been suggested to mitigate this problem, including the introduction of a helium background gas,[15] the application of a fast shutter system,[8] and the use of a tape-drive target system.[7] As far as we know, none of these has succeeded to date.

The debris damage to the x-ray optics is the biggest obstacle to the application of laser-produced plasmas as EUV sources for projection lithography. We have experimentally measured and characterized the debris ejected from clean, smooth surfaced, solid metal targets and found that the deposition rates of these targets on nearby collectors is 4–5 orders of magnitude in excess of these stringent lithography requirements, even with low-pressure buffer gas interdiction.[16] Two new concepts have therefore been formulated in an effort to address the debris problem; they are the mass-limited target design and the use of a cryogenic (or volatile) target material. A mass-limited target is, simply stated, a target that is composed of just the minimum number of atoms necessary to produce the plasma at conditions optimized for generating the desired radiation, and it has the geometry to couple the laser light efficiently to the focused laser spot.

A good example of a volatile target is ice water. Liquid water is volatile at room temperature in a vacuum, and most of the debris from this target will have such a high temperature that it will evaporate in a short time before reaching the x-ray optics. Thus this kind of target offers the possibility of meeting the requirement of less than one in 10^5 target atoms being coated onto optical surfaces. Even if water, or hydrogen and oxygen atoms, are deposited, they will eventually be pumped out by the vacuum system. Water droplets have a higher heat capacity and lower vaporization temperature than most of the equivalent-mass metal droplets, which makes it much easier for the water droplets ejected from a plasma to evaporate before they hit the mirror.

There exists a critical radius r_c,[17]

$$r_c = \frac{2\sigma m}{\rho k T} \frac{1}{\ln[P_r(T)/P_s(T)]},$$

where σ is the coefficient of the surface tension, m is the mass of the gas atom, and ρ is the mass density of the droplet, and $P_r(T)$ and $P_s(T)$ are the inside and outside pressures of the droplet, respectively. A droplet having a radius smaller than r_c will tend to evaporate, which makes r_c even smaller and eventually disappear. For a droplet having a radius greater than r_c, initial temperature T_i should satisfy

$$Ti > \frac{CT_b + H_v - (3\alpha/\rho r) + \frac{1}{2}V^2}{C}$$

in order for it to evaporate completely. Here T_m and T_b are the melting and boiling temperatures, respectively, H_v is the latent heat of vaporization, C is the specific heat of the water, α is the coefficient of surface tension, ρ is the material density, and V is the velocity of the ejected particulate. Full vaporization may require an even higher initial temperature for

bigger droplets, because the flight time of the ejected droplet to the mirror surface is probably less than the vaporization time. Constructing a H_2O target with a limited mass will further reduce the residual particles that might get deposited on the mirror.

The combination of the two concepts, the mass-limited cryogenic target, offers an attractive solution to solving the debris problem for a laser-produced plasma as an EUV source. From the requirements discussed in Section 3, the number of oxygen atoms needed in this mass-limited target is 6.5×10^{16}, which corresponds to a 1.3-μg mass of oxygen. In the form of ice water the mass would be 1.5 μg, occupying a volume of approximately 1.5×10^{-3} mm^3 and a spherical volume of approximately 100 μm in size.

4. Material Cost and Handling

The single-shot cost for the target material of a laser-produced plasma EUV source, by most estimations, must fall within the range of $\$10^{-5}$–$\$10^{-6}$.[18] This goal appears to be unreachable for solid metal targets and for tape-drive targets as well. Table 1 shows the unit price and a single-shot cost for most of the materials that might be utilized as a target for a laser-produced plasma EUV source. Taking solid Sn as an example, we see that the unit price for high-purity Sn is approximately \$2.50/g. Our estimated minimum number of 6.5×10^{16} atoms is approximately 1.3×10^{-5} g of Sn, which corresponds to a single-shot cost of $\$3 \times 10^{-5}$. Supplying the raw material itself has already brought the price up beyond the cost limit, without including the unit shot cost for material processing, polishing, and the laser facility. These costs are likely to be many times the raw material costs.

Table 1. Unit Price and Single-Shot Cost of Materials

Z	Material	Dollars/Gram	Cost for Single Shot[a]
3	Li	9.21	7.00 (−6)
4	Be	588.1	4.29 (−4)
12	Mg	1.68	3.27 (−6)
13	Al	0.137	3.01 (−7)
18	Ar	0.0022	9.50 (−9)
26	Fe	0.048	2.20 (−7)
29	Cu	0.03	1.82 (−7)
30	Zn	2.53	1.34 (−5)
36	Kr	0.267	2.40 (−6)[b]
42	Mo	0.48	3.74 (−6)
48	Cd	0.33	2.97 (−6)
49	In	7.22	6.72 (−5)
50	Sn	2.47	2.37 (−5)
54	Xe	1.535	2.16 (−5)[b]
58	Ce	11.52	13.0 (−4)
73	Ta	2.04	3.00 (−5)
74	W	1.5	2.23 (−5)
78	Pt	84.9	1.34 (−3)
79	Au	83.6	1.33 (−3)
81	Ti	23.85	3.95 (−4)
82	Pb	0.586	9.8 (−6)
	H_2O	0.0055	8.00 (−9)[c]

[a]All data from Goodfellow unless otherwise noted.
[b]Data from Liquid Carbonic.
[c]Data from Fisher Scientific.

In addition to the cost, the feeding of solid materials through vacuum walls into the laser-material interaction region, and especially at the high volume rates required for contemplated kilohertz operation, presents a formidable problem. The tape-drive target system[7] has already demonstrated the engineering complexity required to address this problem seriously, and it still suffers from feeding-rate limitations and the batch-loading downtimes potentially unacceptable for production-line application.

The use of injected fluids as targets solves the material handling problem in a simple and elegant way. Smooth and self-healing surfaces can be irradiated without breaking continuity of operation for extended production periods. Moreover, H_2O is an extremely inexpensive and abundant source material. A small pulsed nozzle system could be used to eject liquid water droplets as a mass-limited cryogenic target. For such a system the principal cost may likely be determined by the hardware and not the target material handling and consumption, which is quite the opposite situation from that of the solid metal or metal film targets. We estimate that the cost per shot is $\$5 \times 10^{-7}$ at maximum.

5. Cryogenic Ice-Water Target

As noted above, the cryogenic ice-water target has many advantages that are needed as a laser-produced plasma source for projection lithography in terms of debris, cost, and handling. There are several strong transitions from lithiumlike oxygen near 13 nm, which shows that this target could also have the CE comparable with that of the solid metal target near this wavelength. The optimization of this radiation depends on both laser and target parameters. In Subsection 5.A. we present theoretical simulation results for this radiation from laser-produced plasma, and the experimental results follow in Subsection 5.B.

A. Calculation of X-Ray Emission Spectra

The x rays emitted from a laser-produced plasma depend strongly on the plasma conditions (T_e and n_e), which in turn depend on parameters of the target and the laser used. Those parameters significantly affecting the x-ray generation are the laser wavelength, laser intensity, laser pulse width, and shape, as well as the target materials. Therefore, the capability of theoretically predicting the x-ray emission spectra under different conditions is very important for the selection of the target material and laser system and for the optimization of the parameters for the specific applications and requirements.

We used three codes in our numerical approach to calculate the laser-produced plasma EUV spectra. The one-dimensional Lagrangian hydrodynamics code, MEDUSA, developed at Rutherford Laboratory,[19] is used to model the hydrodynamic processes in the laser-produced plasma. It solves a set of equations,

including the Navier–Stokes equation, Maxwell equations, the continuity equation, and the equation of the state in the plasma, and it treats the laser pulse as a source term in the energy-conservation equation. This code simulates the plasma dynamic variables such as electron temperature, ion temperature, fluid density, and velocity at different plasma positions (cells) and different times by taking the laser wavelength, laser peak intensity, pulse width, and target variables as its input parameters. For a given time step, the plasma at each cell is considered as in a steady state.

Another code is the atomic physics code, RATION, developed by Lee at Lawrence Livermore National Laboratory.[14] It calculates the synthetic radiation spectra from the high-temperature plasma by taking the atomic number of the target material and the plasma parameters (electron temperature T_e and density n_e) as its input parameters, and it calculates the ion population distribution among different ionization stages and the resulting emission spectra from H-like, He-like, and Li-like ions at the given plasma conditions under the assumption of steady state.

Laser-produced plasmas are generally considered to be high-temperature, high-density plasmas. They also possess very high electron temperatures and density gradients near the critical density where most of the x-ray radiation occurs. The schematic representation of the density and temperature profiles for a typical laser-heated planar target is shown in the Fig. 4,[20] where V_{sh} and V_a are the shock and ablation velocity, respectively, and ρ_c is the critical density. This indicates that the direct application of the RATION code to the laser-produced plasma radiation is inappropriate because the steady state could not be achieved throughout the whole plasma region. Thus we need to divide the whole plasma region into many small parts in which the steady-state condition can be locally assumed, and we need to accumulate the radiation from all these small parts to obtain the overall synthetic EUV spectra of a plasma.

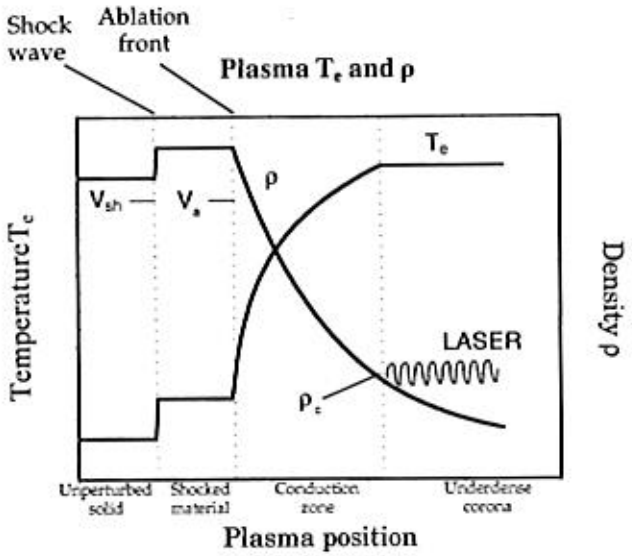

Fig. 4. Schematic representation of electron temperature and density profile for a typical laser-produced plasma.

The simulation of the radiation spectra from a laser-produced plasma for given laser and target conditions therefore requires the integration of MEDUSA and RATION. A third code, WASP, developed at the Laser Plasma Laboratory at the Center for Research and Education in Optics and Lasers (CREOL) serves this purpose. It takes the output of the above two codes as its input data files and produces time- and space-integrated x-ray spectra by using the interpolation method in numerical mathematics. The output of the WASP code can be correlated to measured parameters and compared with the experimental results directly. The current version of the WASP code does not include radiation trapping, i.e., each cell is assumed to be optically thin.

The EUV spectra of the ice target originate mainly from oxygen ions at different ionization stages. The contribution from hydrogen at these regions consists of only weak free-bound continuum emission and is insubstantial relative to the oxygen line emission near 13 nm. The code simulation of the laser plasma radiation is therefore made for an equivalent density and size target of oxygen only. The existence of hydrogen in the ice may cause small changes of the plasma conditions as well as in the x-ray spectra, but it is not expected to be significant in the calculation of the EUV spectra.

There exist four strong line emissions in the 10–20-nm spectral region in an oxygen plasma, which are all generated from electronic transitions in lithiumlike oxygen. They are the transitions of $2s$–$4p$ (11.58 nm), $2p$–$4d$ (12.98 nm), $2s$–$3p$ (15.01 nm), and $2p$–$3d$ (17.30 nm), respectively. The calculated dependence of the four strong lines on laser intensity, wavelength, and pulse width are shown in Fig. 5. Because these four lines all originate from the same ionization stage, they should all follow the same trend with the change of the laser intensity as is in Fig. 5(a). Their intensities increase with laser intensity when $I < 10^{11}$ W/cm^2, and they start to decrease after the intensity reaches 10^{11} W/cm^2. This is due to higher electron temperatures at higher laser intensities, which shifts the optimum population fraction to higher ionization stages (He-like or H-like oxygen ions; see Fig. 2) and reduces the relative population fraction of the lithiumlike oxygen ions.

Figure 5(b) shows the dependence of the x-ray energy output of the four strong lines on the driving laser wavelength for a peak intensity of 10^{11} W/cm^2 and a pulse width of 10 ns. In this simulation, frequency-doubled or frequency-tripled Nd:YAG radiation produces a slightly better result than the fundamental 1.06 μm, but the difference is minor. Though for a given laser intensity the shorter-wavelength laser light is more strongly absorbed by the plasma than that of the longer-wavelength laser because of the relatively high critical density, the increased absorption will most probably shift the population distribution to optimize at higher ionization stages,

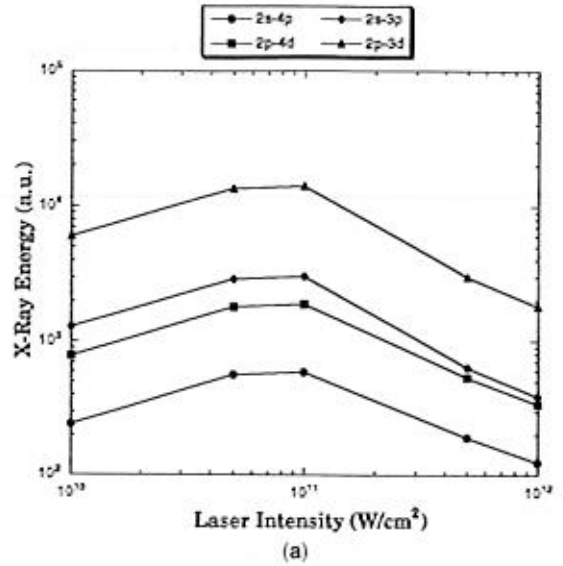

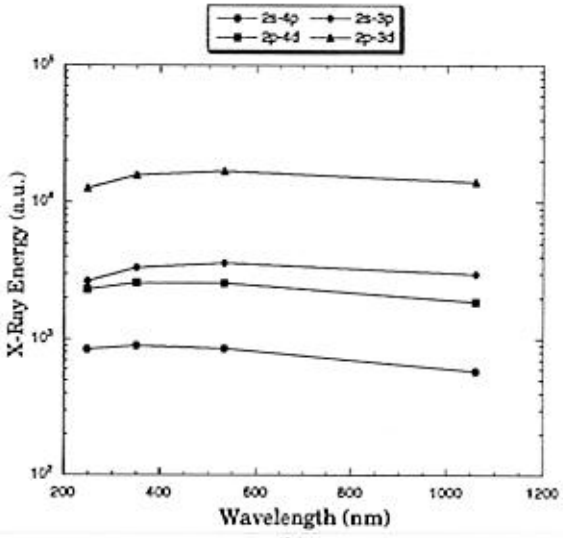

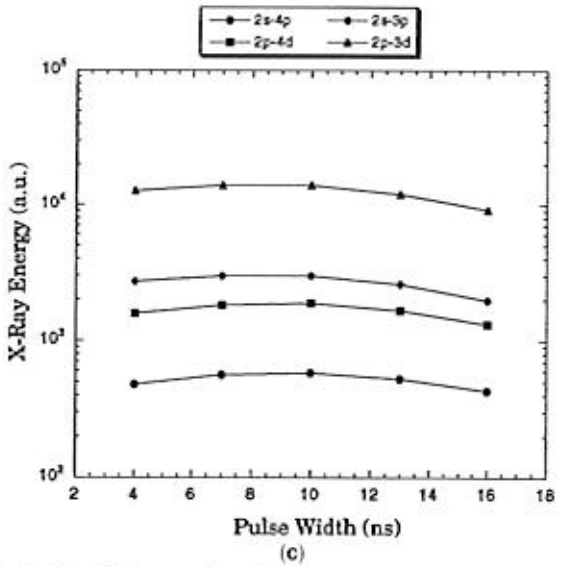

Fig. 5. Simulation results of four strong x-ray lines. Calculated dependence on (a) laser intensity, (b) wavelength, (c) pulse width.

which is similar to the case in the increase of the laser intensity. It seems that the double-frequency or triple-frequency YAG or glass laser would be better than the fundamental frequency in this simulation, but if we also consider the efficiency of the frequency doubling or tripling, then the infrared 1.06 μm may be a better choice.

Because the thermal equilibrium time of the electrons in the plasma is of the order of 1 ps or less, and the change of pulse width in our simulation is of the order of nanoseconds, the plasma temperature and density are not much affected by the pulse width and likewise the radiation spectra. The effect on the x-ray energy of increasing the laser energy by increasing the pulse width is canceled out by the slow deposition rate and the shift of the optimum population, thus keeping the x-ray energy almost unchanged. The x-ray intensities of these four lines do not change appreciably with the laser pulse width up to 20 ns at a fixed peak laser intensity, as is clearly shown in Fig. 5(c). Here the calculations assume a Gaussian temporal shape of the laser pulse. When the laser intensity is fixed, the change of the pulse width increases the total energy of the laser pulse while decreasing the rate of energy deposition.

The above simulation results provide us an indication of how the x-ray radiation changes with the laser parameters and guide us on how to direct our experiment in order to obtain the optimized radiation for our specific application.

B. Experimental Study of the Ice Target

We have recorded soft x-ray spectra of laser-produced plasmas from a bulk ice target at different laser intensities and laser energies. For these measurements we kept the laser wavelength and pulse duration fixed, and we varied the pumping energy and focus conditions. The spectra were compared directly with our simulations described above. The experimental results also serve as a test tool for the validity of the assumptions made in the codes (e.g., steady state, one dimensional, and no radiation trapping). The debris from the bulk ice target was also measured.

1. Experimental Facility

The experimental facility we constructed to analyze the x-ray and plasma emission characteristics of the target is shown in Fig. 6. X-ray emission from the plasma is currently being analyzed with an array of instruments. These include specially calibrated soft x-ray diode (XRD) detectors with a double-reflection multilayer and filter combination, which has sensitivity only within a narrow (0.3-nm) band in the vicinity of 13 nm. High-resolution (6-Å/mm) soft x-ray spectra are recorded by the use of a flat-field grating spectrograph. Other instruments that are designed to measure harder x-ray emission include a pinhole camera used to photograph the plasma region and filtered P-I-N diode detectors (not shown) to determine the time duration of the high-energy x-ray

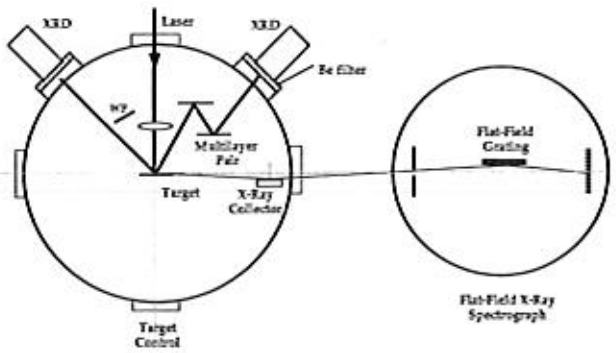

Fig. 6. Experimental setup for x-ray measurement.

emission. A clean silicon wafer witness plate (WP) was put several centimeters away from the laser focal spot, and the debris from the target was collected on it.

A 5-J, 10-ns laser pulse ($\lambda = 1.06$ μm) from a Nd:glass laser was focused onto the target with a $f/5.6$ lens. The setup of the laser oscillator–amplifiers is shown in Fig. 7. This system has several unique characteristics[21]: (a) the seed-injection technique provides single-wavelength oscillation in the system and ensures the uniform beam distribution and a reproducible, Gaussian pulse; (b) a novel four-pass amplification scheme was used to extract most efficiently the stored energy in the active medium; and (c) a phase-conjugation mirror, using stimulated Brillouin scattering (SBS), acts to improve the beam quality of the amplified pulse. A maximum intensity of $\sim 10^{12}$ W/cm^2 was obtained from this system within an approximately 200-μm-diameter spot size. The optimum focal condition was monitored by the aluminum-filtered P-I-N diode because the intensity of the hard x-ray radiation of the plasma depends strongly on the laser intensity. Reagent-grade pure water frozen in a plastic container was used as the ice target. Soft x-ray spectra were recorded with the flat-field grating x-ray spectrograph on Kodak 101-07 film, which was then digitized by use of a densitometer to get the optical density on the film. This optical density was transferred to the x-ray energy per unit area by the film-calibration data given by Henke and co-workers[22,23] and the calculated grating efficiency curve.

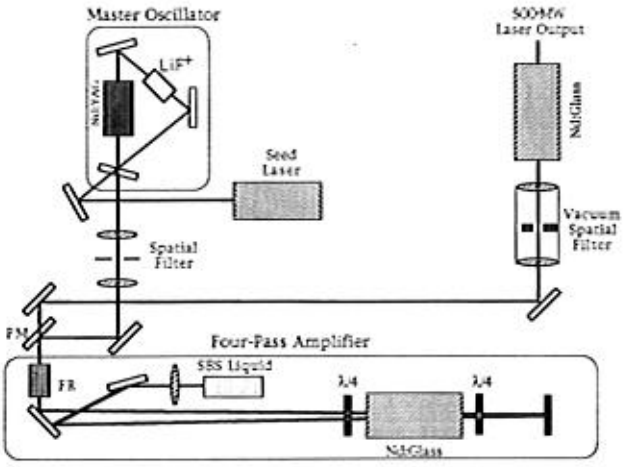

Fig. 7. Seed-injected 500-MW Nd:YAG laser system: PM, polarization mirror; FR, Faraday rotator.

2. *EUV Spectra*

A typical ice spectrum in the region of 5–20 nm is shown at the top of Fig. 8(a), and a synthetic spectrum from our code simulation is shown at the bottom of the figure. The overlap of both spectra in this region and the relative intensities of the four lines show that our spectrograph is well aligned and the assumptions we made in the simulation are seemingly reasonable. Figure 8(b) shows both tin and ice radiation near 13 nm together with a Gaussian reflectivity curve of a Mo–Si multilayer reflective mirror peaked at 13 nm with a bandwidth of 0.3 nm. The ratio of the overlap between the ice spectra and the Gaussian curve to the overlap between the tin

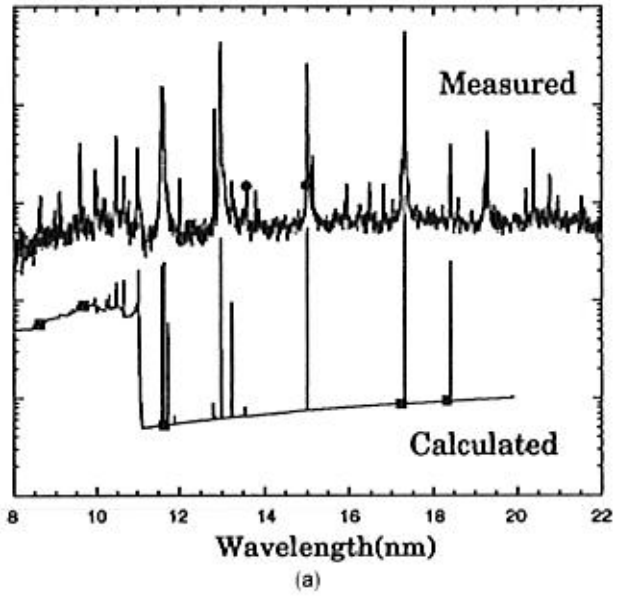

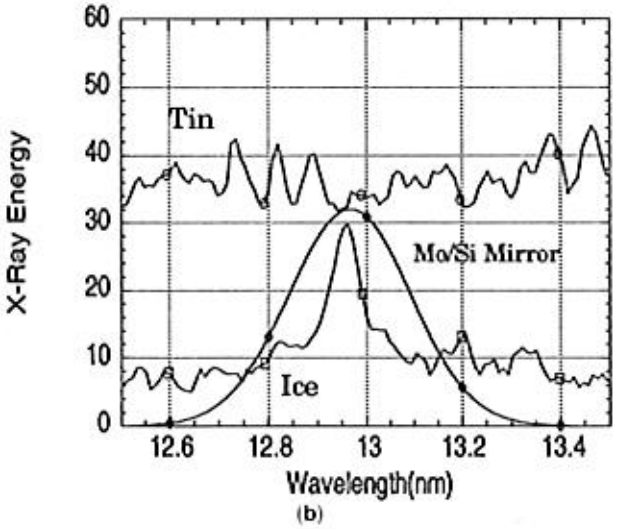

Fig. 8. Calculated and measured x-ray spectra: (a) ice and synthetic spectra, (b) tin and ice radiation.

spectra and the Gaussian curve is 57%, which indicates that the energy CE of the ice-water target is within a factor of 2 compared with that of a solid tin target.

The dependence of the four strong x-ray line emissions on the incident laser intensity and energy is shown in Fig. 9. The variation of the x-ray energy of these strong line emissions with the pump laser energy is shown in Fig. 9(a). The $4d$–$2p$ radiation increases with the laser energy up to 18 J, the maximum energy generated from our laser, whereas the other three lines start to saturate or decrease after ~13 J. Figures 9(a) and 9(b) suggest that the optimum laser intensity is between 10^{11} W/cm^2 and 5×10^{11} W/cm^2. We measured the intensity dependence by changing the laser spot size on the target while keeping the total laser energy constant. The experimental results agree well with the theoretical simulation shown in Fig. 5. The relative variations of the four strong EUV line intensities might be due to the relatively different population distribution among the excited levels of lithiumlike oxygen and the different self-absorption of the radiation by the plasma, which is omitted in the simulation.

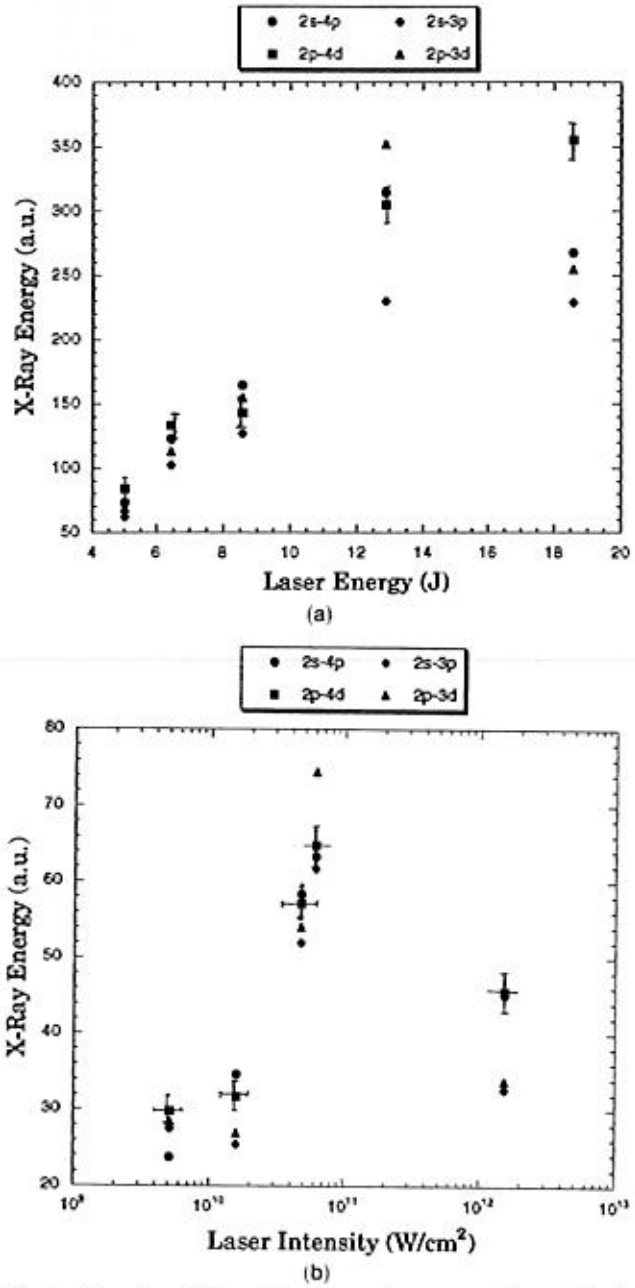

Fig. 9. Experimental results of four strong x-ray lines. Variation with (a) laser energy, (b) laser intensity.

3. *Debris Measurement*

Debris from a laser plasma is in the form of electrons, ions, and neutral atoms from the interaction region, and larger clusters of target material emanating from the resulting shocks and thermal waves into the bulk material. In these experiments, we made debris measurements by putting a silicon wafer some distance in front of the target as a WP.[24] These measurements permitted a detailed analysis of the character of the debris and an estimation of the total mass of debris that would be deposited on the first collecting mirror of a candidate EUV lithography system. Prior to exposure to the emitted laser plasma particulate, the wafer was cleaned and checked under a microscope to ensure that there was no preexisting debris or damage. Because some of the particulate debris has a velocity greater than 9000 cm/s,[24] it has sufficient kinetic energy to damage the silicon wafer locally or to remain adhered to it. After exposure to many laser plasma shots, the wafer was examined with both an optical microscope and an atomic force microscope. WP tests were made for both the Sn and ice-water targets, permitting a comparison to be made with earlier detailed measurements.[24] A typical picture of the wafer after exposure to 100 laser shots with a solid, Sn target taken with an optical microscope is shown in Fig. 10(a). The debris on the wafer appears in different sizes, and much of it is donut shaped. Figure 10(c) is a cross section of the thickness of one of these depositions obtained with an atomic force microscope. It is clear from this picture that the particulate is in liquid form (aerosol) before it reaches the WP. Much of the debris from a Sn target appears in this form; the diameters of the deposited splattered aerosols range from <1 μm to several hundred micrometers. The accumulated buildup of these depositions would efficiently coat a multilayer mirror with material of several tens of a nanometers, thus rendering it ineffective in a relatively small number of laser shots.

The features recorded on a WP for an ice target were markedly different. The only feature evident on the WP after many hundreds of shots was in the form of small impact scars and pits, which is shown in Fig. 10(b). The distribution of these impact scars was highly nonuniform and very sparse. The aerial density was ~400/cm^2 for the same irradiating conditions as for tin, which shows 3 ~ 4 orders of magnitude improvement over the solid tin target. These features probably resulted from heating of the

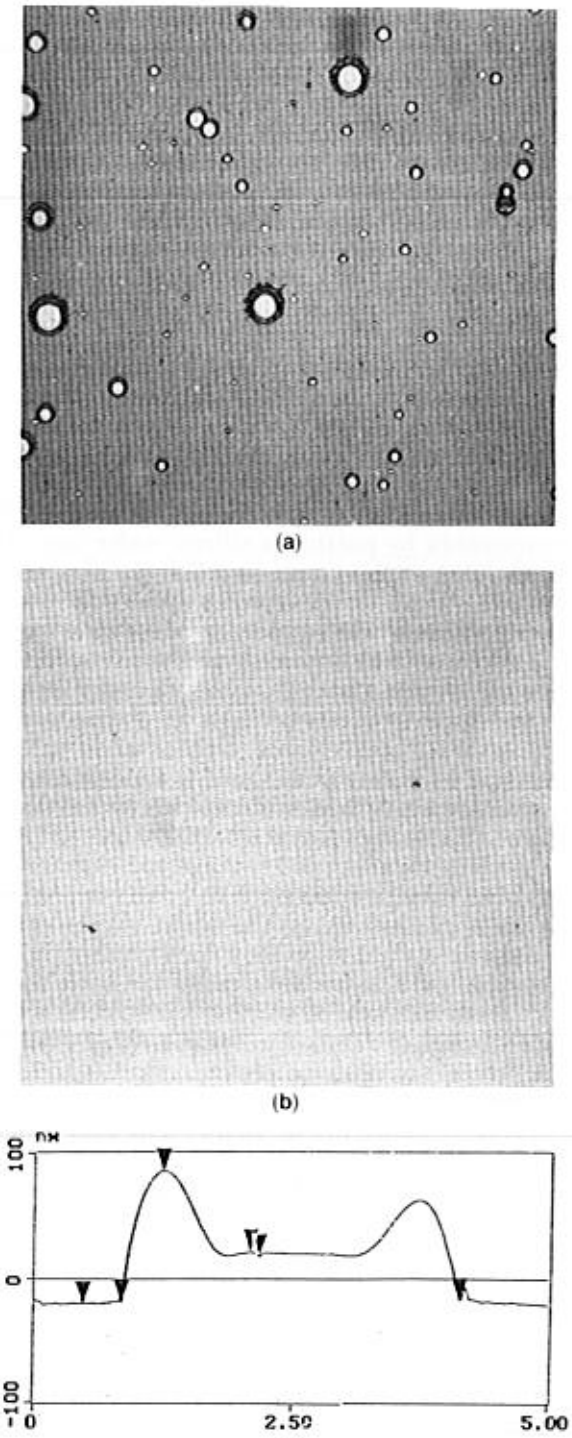

Fig. 10. Debris from tin and ice targets: (a) tin target, (b) ice target, (c) cross section of thickness.

silicon wafer by the high-temperature particles or from steam ejected from the ice target after the laser pulse. When the WP was moved to 7.5 cm from the target, however, nothing could be collected on the silicon wafer. This indicates that much of the ejected material from the ice target evaporates in the vacuum chamber before it reaches the WP. This suggests that 10 cm might be a safe distance to put the collecting optics in the projection lithography system from a solid ice target. Moreover, the use of mass-limited ice targets will eliminate the generation of large particulate ejecta all together.

6. Summary

We developed a cryogenic ice-water target to be used as a bright laser plasma EUV source for application in EUV projection lithography. This target uniquely combines the features of high spectral brightness, low residual radiation, extremely low cost, and low-to-negligible target debris ejection. These source features are necessary for the credible design of production manufacturing facilities producing 0.1-μm-scale circuits. The material cost of the ice target for a single shot is 3–4 orders of magnitude less than the estimated requirement. We calculated the synthetic EUV spectra of the laser-produced plasma based on the MEDUSA and RATION codes and the WASP code that we developed at CREOL. The initial experimental results performed on the cryogenic ice target agree well with our theoretical prediction. Our measurements show that the x-ray radiation within the 0.3-nm bandwidth near 13 nm from the ice target is 57% of that from a solid tin target, and that the debris reduction is at least three orders of magnitude less compared with that of the tin target. Future investigations will concentrate on the use of mass-limited water drop targets in an attempt to reduce debris quantities further, to reduce the handling costs, and to run the system continuously for a relatively long uninterrupted period to demonstrate the practical utility of the target for production-line applications.

The authors thank G. Shimkaveg, D. Salzmann, K. Gabel, and M. Kado of the Laser Plasma Laboratory at CREOL for helpful discussions, and C. Abbott and C. Brown of the Space Science Division of the Naval Research Laboratories for their assistance in digitizing our x-ray spectra. This research was supported by the Advanced Research Projects Agency through contracts with the Lawrence Livermore National Laboratory and Sandia National Laboratory and by the State of Florida.

References and Notes

1. W. T. Silfvast, M. C. Richardson, H. Bender, A. Hanzo, V. Yanovsky, F. Jin, and J. Thorpe, "Laser-produced plasmas for soft x-ray projection lithography," J. Vac. Sci. Technol. B **10,** 3126–3133 (1992).
2. R. L. Kauffman, D. W. Phillion, and R. C. Spitzer, "X-ray production ~ 13 nm from laser-produced plasma for projection x-ray lithography application," Appl. Opt. **32,** 6897–6900 (1993).
3. O. R. Wood II, J. E. Bjorkholm, J. Boker, L. Eicher, R. R. Freeman, T. E. Jewell, W. M. Mansfield, A. A. MacDowell, L. H. Szeto, D. M. Tennant, W. K. Waskiewicz, D. L. White, and D. L. Windt, "High-resolution soft x-ray projection imaging," in *Soft-X-Ray Projection Lithography,* J. Bokor, ed., Vol. 12 of OSA Proceedings (Optical Society of America, Washington, D.C., 1991), pp. 40–42.
4. A. G. Michette, "X-ray microscopy," Rep. Prog. Phys. **51,** 1525–1604 (1988).

5. A. M. Hawryluk and L. Seppala, "Soft x-ray projection lithography using an x-ray reduction camera," J. Vac. Sci. Technol. **6**, 2162–2166 (1988).
6. F. Jin, K. Gabel, M. Richardson, M. Kado, A. F. Vasil'ev, and D. Salzmann, "Mass-limited laser plasma cryogenic target for 13 nm point x-ray sources for lithography," in *Applications of Laser Plasma Radiation*, M. C. Richardson, ed., Proc. Soc. Photo-Opt. Instrum. Eng. **2015**, 151–159 (1993).
7. S. J. Haney, K. W. Berger, G. D. Kubiak, P. D. Rockett, and J. Hunter, "Prototype high-speed tape target transport for a laser plasma soft-x-ray projection lithography source," Appl. Opt. **32**, 6934–6937 (1993).
8. M. S. Schulz, A. G. Michette, and R. E. Burge, "A study of the feasibility of x-ray microscopy with a laser-plasma source," in *X-Ray Microscopy III*, A. G. Michette, G. Morrison, and C. Buckley, eds. (Springer-Verlag, Berlin, 1992), p. 58.
9. M. Richardson, K. Gabel, F. Jin, and W. T. Silfvast, "Cryogenic targets for laser plasma x-ray lithography," in *Soft X-Ray Projection Lithography*, A. M. Hawryluk and R. H. Stulen, eds., Vol. 18 of OSA Proceedings (Optical Society of America, Washington, D.C., 1993), pp. 156–162.
10. M. C. Richardson, K. Gabel, M. Kado, and F. Jin, "Water laser plasma x-ray point source and apparatus," U.S. patent pending (1994).
11. N. M. Ceglio and A. M. Hawryluk, "Soft x-ray projection lithography system design," in *Soft-X-Ray Projection Lithography*, J. Bokor, ed., Vol. 12 of OSA Proceedings (Optical Society of American, Washington, D.C., 1991), pp. 5–10.
12. R. C. Spitzer, R. L. Kauffman, T. Orzechowski, D. W. Phillion, and C. Cerjan, "X-ray production from laser produced plasmas for SXPL application," in *Soft X-Ray Projection Lithography*, A. M. Hawryluk and R. H. Stulen, eds., Vol. 18 of OSA Proceedings (Optical Society of America, Washington, D.C., 1993) pp. 142–145.
13. Data derived from the SPECTRA database created by A. Ya. Falenov and I. Ya. Skobelev (1993).
14. R. Lee, *User Manual for* RATION (University of California and Lawrence Livermore National Laboratory, Livermore, Calif., 1990).
15. I. C. E. Turcu, G. J. Tallents, M. S. Schulz, and A. G. Michett, "High repetition rate laser-plasma x-ray source for microscopy," in *X-ray Microscopy III*, A. G. Michette, G. Morrison, and C. Buckley, eds. (Springer-Verlag, Berlin, 1992), p. 54.
16. M. Richardson, W. T. Silfvast, H. A. Bender, A. Hanzo, V. P. Yanovsky, F. Jin, and J. Thorpe, "Characterization and control of laser plasma flux parameters for soft-x-ray projection lithography," Appl. Opt. **32**, 6901–6910 (1993).
17. K. Huang, *Statistical Mechanics*, 2nd ed. (Wiley, New York, 1987), Chap. 2, p. 36.
18. A. M. Hawryluk and N. M. Ceglio, "Wavelength considerations in soft x-ray projection lithography," Appl. Opt. **32**, 7062–7067 (1993).
19. P. A. Rodgers, A. M. Rogoyski, and R. S. Y. Rose, *MEDIOI: A Laser-Plasma Simulation Code*, User guide (Appleton, Rutherford, N.J., 1989).
20. R. Fabbro, C. Max, and E. Fabre, "Planar laser-driven ablation: effect of inhibited electron thermal conduction," Phys. Fluids **28**, 1463–1481 (1985).
21. V. P. Yanovsky, M. C. Richardson, and E. J. Miesak, "Compact, single-frequency, high-power Nd:glass laser," IEEE J. Quantum Electron. **30**, 884–886 (1994).
22. B. L. Henke, F. G. Fukiwara, M. A. Tester, C. H. Dittmore, and M. A. Palmer, "Low-energy x-ray response of photographic films. II. Experimental characterization," J. Opt. Soc. Am. B **1**, 828–849 (1984).
23. B. L. Henke, S. L. Kwok, J. Y. Uejio, H. T. Yamada, and G. C. Young, "Low-energy response of photographic films. I. Mathematical models," J. Opt. Soc. Am. B **1**, 818–827 (1984).
24. W. T. Silfvast, H. Bender, A. M. Eligon, D. O'Connell, A. Hanzo, and M. C. Richardson, "Laser plasma source characterization for SXPL," in *Soft X-Ray Projection Lithography*, A. M. Hawryluk and R. H. Stulen, eds., Vol. 18 of OSA Proceedings (Optical Society of America, Washington, D.C., 1993), pp. 117–126.